



1 Multiconfiguration electromagnetic induction survey for paleochannel internal structure
2 imaging: a case study in the alluvial plain of the river Seine, France.

3

4 Fayçal Rejiba⁽¹⁾, Cyril Schamper⁽¹⁾, Antoine Chevalier⁽¹⁾, Benoit Deleplancque⁽²⁾, Gagahik
5 Hovhannissian⁽³⁾, Julien Thiesson⁽¹⁾ & Pierre Weill⁽⁴⁾

6

7 ⁽¹⁾*Sorbonne Universités – UPMC Univ Paris 06, CNRS, UMR 7619 METIS, Paris, France*

8

⁽²⁾*MINES ParisTech, France*

9

⁽³⁾*Centre IRD France Nord, – UMR 242 - IEES Paris, Bondy, France*

10 ⁽⁴⁾*Normandie Univ, UNICAEN, CNRS, Morphodynamique Continentale et Côtière, 14000
11 Caen, France*

12 *Corresponding author: Fayçal Rejiba (faycal.rejiba@upmc.fr)*

13 *Running title: Geophysical Investigations of a Paleochannel*

14

15

16

17

18



19 **Abstract**

20 The La Bassée floodplain area is a large groundwater reservoir controlling most of the water
21 exchanged between local aquifers and hydrographic networks within the Seine River Basin
22 (France). Preferential flows depend essentially on sediment fills, whose characteristics are
23 strongly influenced by paleomeander heterogeneities. A detailed knowledge of the internal
24 heterogeneities of such paleomeanders can thus lead to a comprehensive understanding of its
25 long-term hydrogeological processes. A geophysical survey based on the use of
26 electromagnetic induction was performed on a representative paleomeander, situated close to
27 the city of Nogent-sur-Seine in France. In the present study we assess the advantages of
28 combining several spatial offsets, together with both vertical and horizontal dipole
29 orientations (6 apparent conductivities), thereby mapping not only the spatial distribution of
30 the paleomeander derived from LIDAR data, but also its vertical extent and internal
31 variability.

32

33 **1 – Introduction**

34 Dipolar source electromagnetic induction (EMI) techniques are frequently used for critical
35 zone mapping, which can be applied to the delineation of shallow heterogeneities, thereby
36 improving conceptual models used to explain the processes affecting a wide range of
37 sedimentary environments. This mapping technique is very effective for environments in
38 which the spatial structure has strongly contrasted electromagnetic (EM) properties, especially
39 that of electrical conductivity. The clay infilling of paleochannels, and the deposition of
40 alternate layers of fine (conductive) and coarse (resistant) material in alluvial plain systems,
41 are examples of natural geophysical processes having contrasted EM properties.



42 EMI measurements have previously been applied to the imaging of fine-grained
43 paleomeander infilling, produced by meander neck cutoff or river avulsion, which can form
44 permeability barriers with complex geometries (e.g. Miall, 1988; Jordan and Prior, 1992). In
45 addition to providing detailed local information on alluvial plain heterogeneities, which can
46 be applied to the study of aquifer-river exchanges, the estimation of the geometry of the Seine
47 river can provide valuable insight into its paleo-hydrology, as well as physical transformations
48 resulting from climatic fluctuations during the Late Quaternary.

49 EMI devices are increasingly used for a large number of near-surface geophysical
50 applications, as a consequence of their ability to produce 2D images of the apparent electrical
51 conductivity, σ , over a large surface. A very large body of scientific literature has been
52 dedicated to the study and use of near-surface electromagnetic geophysics, especially in the
53 frequency domain, as described by Everett (2012).

54 By design, an EMI system energizes a transmitter coil with a monochromatic
55 oscillating current, and the oscillating magnetic field produced by this current induces an
56 oscillating voltage response in the receiver coil. The voltage response measured in the
57 absence of any conductive structure is used as a standard reference. However, the magnetic
58 field oscillations are distorted by the presence of nearby conductive structures, such that the
59 voltage signal induced in the receiver coil experiences a shift in amplitude and phase with
60 respect to that observed in the standard reference. This shift can be conveniently represented
61 by a complex number, comprising quadrature and in-phase (respectively, real and imaginary)
62 components, which can be inverted and then interpreted in terms of an apparent conductivity
63 and an apparent depth of investigation (DOI).



64 Although EMI systems were initially used as mapping tools, and were designed to
65 measure the lateral variability of σ associated with a single apparent DOI, the measurements
66 they provide are now generally interpreted to provide information as a function of depth,
67 albeit down to relatively shallow depths only. This interpretation relies on the fact that, for a
68 given soil model, one specific apparent DOI is defined by three device setup parameters: (1)
69 the offset between the transmitter and receiver magnetic dipole, (2) the orientation of the
70 dipole pair, and (3) the frequency of the transmitter current oscillations. An EMI survey
71 during which at least one of these parameters is varied can thus be used to resolve depth-
72 related variations of conductivity. The real (as opposed to the apparent) DOI is determined
73 from the computed distribution of the ground's electrical properties. This distribution can be
74 retrieved by solving an inverse problem, which is derived from a large number of applications
75 (e.g. Tabbagh, 1986; Spies, 1989; Nabighian, 1988; Schamper et al., 2012).

76 The physical model used in the inversion procedure must be suitably adapted to the
77 electromagnetic properties of the surveyed ground. In the case of a medium characterized by
78 typical conductive properties, at a low induction number the quadrature response is
79 interpreted in terms of the apparent ground resistivity, which to a first order approximation
80 varies linearly with the quadrature response (McNeill, 1980). In a resistive or highly
81 conductive environment, such as that presented in the present study, the McNeill equation is
82 no longer valid, and EMI recordings, in particular their in-phase component, must be
83 interpreted within the specific measurement context, taking all of the physical properties of
84 the local environment into account (e.g. Simon et al., 2015; Benech et al., 2016).

85 The present study focuses on the alluvial plain of La Bassée, a zone located in the
86 southern part of the Seine basin, 2 km to the west of Nogent-sur-Seine (France). The aim of
87 this study is to delineate the geometry of a paleochannel (i.e. its thickness and width), using a



88 state-of-the-art 1D inversion routine applied to EMI apparent conductivity measurements. The
89 inverted data consists in a set of EMI measurements implemented with (1) three different
90 offsets, for two dipole configurations: horizontal (HCP) and vertical (VCP).

91 Following a description of the study area, we present the technique used to calibrate
92 the EMI measurements, which relies on reference ERI (Electrical Resistivity Imaging)
93 measurements and an auger sounding profile. The EMI inversion is then constrained to limit
94 the solution space to images that are consistent with the observations provided by the ERI and
95 auger soundings. To this end, a local three-layer model is derived with fixed conductivities,
96 and is then introduced into the inversion routine for each position of the surveyed area. The
97 thicknesses of the soil and conductive filling, corresponding to the presumed paleochannel,
98 are determined through the use of an inversion algorithm.

99 **2- Description of the study area**

100 The study site is located within a portion of the Seine river alluvial plain (locally named “La
101 Bassée”), approximately one hundred kilometers upstream of Paris (France), between the
102 confluence of the Seine and Aube rivers to the North-East, and the confluence of the Seine
103 and Yonne rivers to the South-West (Figure 1). This 60 kilometer-long, 4 kilometer-wide
104 alluvial plain constitutes a heterogeneous sedimentary environment, resulting from the
105 development of the Seine River during the Middle and Late Quaternary. It is important to
106 fully characterize a river’s alluvial plain geometry, in order to understand the fluvial system’s
107 response to climatic fluctuations. More practical issues related to water resource management
108 require an accurate understanding of the exchanges that took place between the regional
109 aquifer and the superficial hydrosystem (Flipo et al. 2014).



110 Cartographic studies of this area have been carried out in the past, using
111 geomorphological and sedimentological techniques (Mégnyen, 1965; Caillol et al., 1977;
112 Mordant, 1992; Berger et al., 1995; Deleplancque, 2016), thus allowing the broad-scale
113 distribution and chronology of the location of the main Middle and Late Quaternary alluvial
114 sheets to be estimated.

115 In addition, the French Geological Survey (BRGM) has compiled a database of more
116 than 500 soundings, which are uniformly distributed over the Bassée alluvial plain, and most
117 of which reached the cretaceous chalky substrate. A detailed analysis and interpretation of this
118 database has allowed the substratum morphology to be reconstructed, the alluvial infilling
119 thickness to be evaluated, and a preliminary quantitative analysis of the sedimentary facies
120 distribution to be determined (Deleplancque, 2016). The maximum thickness of the alluvial
121 infilling is thus known to lie between 6 and 8 m.

122 Geophysical investigations of gravel pits (after removal of the conductive topsoil)
123 were carried out using ground-penetrating radar (Deleplancque, 2016), and have contributed
124 to the characterization of the sedimentary contrast of the sand bar architecture, between the
125 Weichselian and Holocene deposits. The Weichselian deposits are typical of braided fluvial
126 systems, with fluvial bars of moderate extent (< 50 m) truncated by large erosional surfaces.
127 The thickness of the preserved braid-bars rarely exceeds 1.5 m. The Holocene architecture is
128 associated mainly with single-channel meandering fluvial systems, characterized by thick
129 point-bar deposits (> 4 m) with a lateral extent of several hundred meters, sometimes
130 interrupted by clayey paleochannel infillings. Traces of small sinuous channels, probably
131 using the paths of former Weichselian braided channels, are also identified at the edge of the
132 alluvial plain.



133 Aerial photography and a LIDAR topographic survey (Figure 2) have been used to
134 characterize the paleochannel plan-view morphologies (style, width, meander wavelength), of
135 the most recent (Holocene) meandering alluvial sheets in this area (Deleplancque, 2016).
136 These measurements were complemented by auger soundings and ¹⁴C dating of organic debris
137 or bulk sediment (peat), in order to determine a time-frame for the development of the Seine
138 meanders, to allow this changes to be compared with other regional studies (e.g. Antoine et al.
139 2003; Pastre et al., 2003). The paleochannel investigated in this study is located 2 km to the
140 South-West of Nogent-sur-Seine, and is characterized by larger dimensions than the present-
141 day Seine river. Its width is estimated to lie between 150 and 200 m, with a meander
142 wavelength between 2 and 3 km. According to the alluvial sheet analysis and the dating of
143 organic material in the mud-plug of the abandoned meander, it is very likely that this
144 paleochannel was active between the Late Glacial and Preoboreal periods.

145 The main objective of the present study is to refine the lateral extent, and to determine
146 the depth of this paleochannel. The use of geophysical exploration for this investigation is of
147 significant importance, since it should pave the way towards paleo-hydrological
148 reconstruction of the Seine river (estimation of its cross-sectional geometry and paleo-
149 discharge).

150

151 **3 - Methodology**

152 *3.1 Measurement setup*

153 The survey coordinates were determined through the use of a LIDAR map, combined with the
154 analysis of a series of auger soundings made along a reference transect almost 400 m in length
155 (Figure 2, Figure 3). The lateral extent of the meander was delineated using an



156 electromagnetic induction system (CMD explorer) produced by GF instruments s.r.o., with
157 non-regular gridding and non-perfect overlapping inside the same area.

158 The identification of Holocene clay infilling along this reference profile was confirmed by
159 measuring several electrical resistivity profiles (ERI), along the reference transect. For this, a
160 Wenner-Schlumberger array was selected, with 48 electrodes positioned at a 1 m spacing for
161 the first 340 m, and a 0.5 m spacing thereafter.

162 ElectroMagnetic Induction (EMI) surveys were carried out using a CMD explorer (GF
163 instruments), with vertical (Horizontal CoPlanar - HCP) and horizontal (Vertical CoPlanar -
164 VCP) magnetic dipole configurations. The CMD explorer operates at 10 kHz, and allows
165 simultaneous measurements to be made with three pairs of Tx-Rx coils, using a single
166 orientation (T-mode). Three different offsets were used between the centers of the Tx and the
167 Rx coils, namely: 1.48 m, 2.82 m and 4.49 m, each corresponding to a distinct DOI. As the
168 VCP and HCP surveys were made separately, slightly different sampling intervals were used.
169 In addition, GPS reception difficulties led to several gaps in the VCP and HCP surveys. It was
170 thus important to carefully evaluate these shortcomings, before attempting to merge the HCP
171 and VCP measurements during the inversion. As the CMD allows the user to export raw out-
172 of-phase data (including the factory calibration only), no pre-processing is needed to obtain
173 the value of the ratio between the secondary and primary magnetic field amplitude.

174 *3.2 Auger sounding results*

175 A total of 13 hand auger soundings down to a maximum depth of 2.4 m (Figure 4), were made
176 along the reference profile. Some of these soundings did not reach the base of the
177 paleomeander mud-plug (clay / gravel transition), suggesting that the maximum depth of the
178 paleomeander is greater than 2.4 m. The auger soundings revealed the presence of two main



179 units. The uppermost unit is comprised of topsoil, which overlies a layer of loam containing a
180 significant proportion of gravel and sand in the eastern part of the reference profile portion of
181 the paleochannel. A clayey layer, the bottom of which was not reached in the deepest portion
182 of the paleochannel, is situated below this unit. In some soundings, the clayey facies contains
183 layers of peat (PTA, 04, 05, 08, and 09, in Figure 4).

184 *3.3 ERI results*

185 The ERI cross-section (Figure 5) is produced using a dataset of more than 5000
186 measurements. In order to estimate the true resistivity distribution, the resulting apparent
187 resistivity sections were processed by means of inverse numerical modeling, using the
188 Res2dinv software (Loke et al., 2003) with its default damping parameters, and the robust
189 (L1-norm) method. Following a total of 7 iterations, the resulting ERI profiles had an rms
190 error of 0.48% and 0.93%, for the case of the 1 m and 0.5 m electrode spacings, respectively.

191 The resistivity cross-section reveals two main units: an uppermost conductive unit
192 with a resistivity below 20 Ωm , corresponding to a clayey matrix, and a second, more
193 resistive unit with a resistivity greater than 60 Ωm , associated with a medium/coarse-grained
194 silty horizon. The auger soundings are always achieved by a refusal, which is most likely due
195 to the fact that they had reached the resistive second unit. When compared to the analysis
196 achieved using auger soundings, the electrical properties of the topsoil/loam formation appear
197 to be merged with the clayey formation, with the exception of the western portion of the
198 cross-section, which has significant sand and gravel content. This outcome could also be due
199 to the finer spatial resolution of the ERI measurements (electrode spacing of 0.5 m).

200 *3.4 EMI calibration from ERI*



201 Apparent electrical conductivities measured using EMI are particularly sensitive to the
202 orientation of the device, the height above the ground at which the EMI system is installed
203 during the survey, and the 3D variability of the conductivity. In addition, for the interpretation
204 of the measurements, the ground is assumed to be horizontally layered at any given location,
205 even for the smallest dipole offset. Although the orientation (vertical or horizontal) and height
206 of the dipole are initialized at the beginning of each survey, the noise associated with the
207 measurements is related to the near surface variability and in a certain way to variations in
208 orientation and height of the EMI device during acquisitions.

209 In order to improve absolute (not relative) evaluation of EMI data, in situ calibration
210 of EMI data is important. Ideally, calibration must be performed for several heights and over a
211 perfectly known half space which electromagnetic properties spanned over a representative
212 range of conductivity values. For the CMD instrument, calibration factors are provided by the
213 manufacturer for 0 (laid on ground) and 1 m heights. However those factors are valid for a
214 given conductivity range and are dependent on the prospection height (which is never exactly
215 1 m). This height effect, as mentioned above, has a relative stronger influence on the shortest
216 offsets; consequently, to improve the absolute estimation of the apparent conductivity, it is
217 important to have a reference zone where the ground is very well constrained. A series of
218 hand-made auger soundings were used to obtain reliable direct observations down to a depth
219 of 2 m. It shows that the interface between the silty clay and the gravel corresponds to the
220 conductive filling; this was observed at some of the auger sounding locations, namely
221 soundings numbered: 01, 02, 03, 10, 11, 12, and 13, which barely attained a depth of 2 m. In
222 order to obtain deeper information, an ERI prospection has been carried out; the inversed ERI
223 section provides reference and absolute values of the local resistivities and can be used in the
224 calibration process as described in Lavoué et al. (2010). It is worth noting that other in situ



225 ways of calibration could be performed, particularly, using the theoretical response of a
226 metallic and non-magnetic sphere (Thiesson et al., 2014).

227 During the field data acquisition we faced several difficulties that prevent us to do a
228 CMD profile exactly on the reference profile. Actually, the EMI data used for the calibration
229 have been taken from the mapped data closest to the reference profile. This has led to several
230 positioning and alignment errors : 1) the EMI data do not exactly cross the reference profile,
231 2) the EMI data are irregularly spaced along the ERI profile, and 3) the orientation of the
232 CMD device was not exactly the same, for each measurement retained for the calibration.

233 In order to compute the apparent conductivity of a layered ground, based on
234 measurements made using a horizontal or vertical magnetic dipole configuration, we used the
235 well-known electromagnetic analytical solution for cylindrical model symmetry, given by
236 (Wannamaker et al., 1984; Ward and Hohmann, 1988; Xiong, 1989). However, in the case of
237 thin layers or high frequency content, convergence problems can be encountered in the
238 numerical integration of the corresponding oscillating Bessel functions. At frequencies below
239 100 kHz, as in the case of the present study, the numerical filters developed by Guptarsarma
240 and Singh (1997) were found to provide an efficient solution to this problem. The inversion
241 scheme developed in Schamper et al. (2012) was used to invert the EMI measurements. For
242 each offset and dipole orientation, a linear relationship (shifting and scaling) is determined
243 between each measured apparent conductivity and the apparent conductivity estimated from
244 the resistivity models (derived from the ERI panel, Figure 6). Once the calibration done, the
245 new EMI inversion matches the ERI used for the calibration which illustrates the validity of
246 the procedure. Actually, despite the linear relationship assessed between the EMI and ERI
247 resistivities, several non-linear operations are applied: (1) ERI local 1D models along the
248 profile are used to simulate EMI measurements, (2) EMI field data are then fitted (linearly) to



249 those simulations using a non-linear optimization procedure to estimate calibration factors, (3)
250 finally the calibrated/shifted data are inverted with a non-linear forward modeling. All those
251 non-straightforward steps imply that a check is necessary to ensure that the calibration process
252 has been correctly applied. Step (3) does not guarantee that estimated interfaces will match
253 the ERT interfaces 1) if the fixed/chosen resistivities are not correct, or 2) if EMI does not
254 integrate the ground in the same way as the ERI in case of strong anisotropy, which seems not
255 to be the case here, since a good match is obtained.

256 The correlation coefficients are comprised between 0.5 and 0.7. Such values can be
257 explained by several sources of errors in the estimation of the EMI apparent conductivities
258 along the reference profile: 1) the differences in the location between the EMI measurements
259 used for the calibration and the ERI profile, 2) the fact that the one dimensional model used
260 for the EMI modeling is extracted from the inversed 2D resistivity section, 3) the difference
261 of sensitivity between the ERI and EMI data. The regressions indicate the need of a stronger
262 correction for the VCP configuration than for the HCP configuration. The scaling correction
263 decreases as a function of offset, particularly for the HCP, which can be explained by the fact
264 that small offsets are more sensitive to positioning and orientation errors, as well as natural
265 near-surface variabilities.

266 *3.5 Inversion parameters*

267 Once the calibration process is completed, the corrected, apparent HCP and VCP
268 conductivities are inverted, following their interpolation (by kriging) onto the same regular
269 grid. The ERI results indicate a two-layer model (but do not highlight the topsoil), while the
270 auger sounding show clearly a topsoil layer of few decimeters thickness above the conductive
271 formation. Consequently, a three-layer model seems reasonably justified all over the site



272 during the inversion process to represent the studied area: a resistive topsoil, a conductive
273 clayey filling, and a resistive sand/gravel layer. The resistivity of each layer corresponds to
274 the peak values of the bimodal histograms of the reference 1-meter-spaced ERI profile, as
275 shown in Figure 7. The topsoil conductivity derived from the half-meter-spaced ERI profile in
276 the eastern portion is found to be very similar to the conductivity of the resistive layer inferred
277 from the 1m-spaced ERI profile; the first and third layer conductivities are thus considered to
278 be equal. This leads to the following model for the mean conductivity of the three layers: $\sigma_1 =$
279 13 mS/m; $\sigma_2 = 72$ mS/m; $\sigma_3 = 13$ mS/m. It should be noted that the CMD explorer is operated
280 at a single frequency (10 kHz). The sounding height was taken to be 1m for all the field
281 measurements.

282 Figure 8 shows the inverted thicknesses of the first and second layers, and the data
283 residual for the HCP (3 offsets), the VCP (3 offsets), and the combined HCP and VCP
284 conductivities (6 apparent values). The standardized root-mean-squared residual for N
285 independent measurements is given by:

$$286 \quad \sqrt{\frac{\sum_{i=1}^N \left(\frac{d(i) - d_{meas}(i)}{std(i)} \right)^2}{N}}$$

287 Where N is the number of data points, d is the forward response of the estimated model at the
288 end of the inversion, d_{meas} contains the data, and std is the stand deviation of the data.

289 The standard deviation std was estimated from repeated measurements at several
290 locations, as 1 mS/m (with a minimum error of 5%).

291

292 4- EMI inversion results and discussion



293 *4-1 General trend*

294 The layer thickness inversion was performed using three different datasets: (1) the HCP
295 dataset, (2) the VCP dataset, and (3) the combined HCP and VCP dataset (Figure 8).

296 Whatever the dataset used for the inversion, the thickness computed for the topsoil
297 formation (indicated by “*Thickness 1*” in Figure 8) is very small (blue), whereas that
298 computed for the conductive infilling (indicated by “*Thickness 2*”) has a significantly higher
299 value (red), and *vice versa*. Although it varies in thickness, the conductive layer formation
300 spans most of the survey area, whereas the resistive topsoil formation varies mainly in two
301 distinct locations: (1) the south-western limit of the surveyed area, where it reaches a depth of
302 2 m and (2) the mid-northern portion of the surveyed area, where its thickness never exceeds
303 0.6 m. In addition, very small scale topsoil formations are scattered over the surveyed area.
304 Nevertheless, all of the observed topsoil formations appear to be correlated with a local
305 increase in data residual. The thickness of the conductive infilling lying below the topsoil
306 formation, ranges between 0 m, in the south-western portion of the studied zone, and its
307 maximum value of almost 2 m at the center of the map.

308 The VCP mode increases the measured thickness of the shallowest portions of the
309 topsoil layer, whereas the HCP mode tends to negate this layer over most of the surveyed area
310 (central part), where it is not extremely thick. This tendency appears to be correlated with a
311 slight increase in the thickness of the second conductive layer.

312 The inversion of all data, in the form of a single dataset, appears to lead to a mixture of
313 the properties inherent to each of the constituent datasets. This outcome is particularly
314 noticeable in the case of the topsoil formation, where certain structures retrieved by both



315 datasets are emphasized with respect to structures that are present in only one or the other of
316 these.

317 *4-2 Internal variability*

318 In addition to strong meander wavelength variations, each dipole orientation reveals different
319 level of heterogeneities in the material present in the conductive fill, as well as the topsoil.
320 Concerning the material close to the surface (< 2 m), this variability is clearly illustrated by
321 the auger soundings, whereas the conductive unit identified by the ERI section is considerably
322 more complex. In simple terms, the thickness of the conductive material tends to decrease,
323 wherever the silty and sandy material reaches the surface.

324 It should be noted that the inversions observed for each dipole orientation are not
325 systematically preserved in the inversion produced by combining the data from both dipole
326 orientations. This result indicates that in the present context, each orientation is
327 complementary, and contributes a specific set of information. This is particularly relevant in
328 the northern portion of the studied area, where the thickness of the first resistive layer is more
329 variable when it is measured with the horizontal dipole configuration (VCP), than with the
330 HCP configuration.

331 The data residual has numerous peaks in the south-western portion of the study zone.
332 In this zone, the resistive topsoil reaches a thickness of 1 m, leading to EMI measurements
333 with a lower sensitivity (and thus lower signal to noise ratio - SNR). The combined
334 HCP&VCP data inversion naturally leads to the occurrence of higher values of data residual,
335 than in the case of the individual HCP or VCP inversions.

336



337 **5- Conclusion**

338 We presented the results of geophysical investigations of a paleochannel in the alluvial plain
339 of La Bassée (Seine basin, France). The location of this paleochannel and its internal
340 variability, suggested by a LIDAR campaign, have been accurately mapped using a multi-
341 configuration (various offsets and orientations) electromagnetic induction device (CMD
342 explorer from GF instruments).

343 In order to correct the sensitivity issues arising from EMI measurements, a calibration
344 procedure was implemented, based on the use of a linear correction with ERI inversion results
345 and auger soundings. The shifting and scaling of EMI HCP and VCP measurements was made
346 for the three available offsets (1.48m, 2.82m and 4.49m), at a frequency of 10 kHz. Six
347 apparent conductivities allowed the inversion of a reliable three-layer model, comprising a
348 conductive filling with a conductivity equal to 72 mS/m below the topsoil, and a resistive
349 substratum having a conductivity equal to 13 mS/m. The conductivities of the three-layer
350 model were adjusted using the bimodal histogram distribution of the reference ERI profile.

351 In conclusion, the inverted thicknesses are characterized by a significant internal
352 variability in the conductive filling and the topsoil, associated with the paleochannel
353 geometry. The joint inversion of multi-offset HCP and VCP configurations leads to a very
354 interesting result, in which the internal variability description is considerably enhanced. We
355 believe that multiconfiguration EMI geophysical survey carried out at an intermediate scale,
356 should provide a great complement to TDR (Time Domain Reflectometry) for a quantitative
357 and physical calibration of remote sensing soil properties and moisture content.

358 Although the generalization of combined VCP and HCP prospection could
359 significantly improve the accuracy of hydrogeological modeling, it would also lead to a



360 substantial increase in survey costs. This option thus remains to be debated during the 7th
361 phase (WP 1: Sedimentary, Morphological, Hydrogeological and Thermal properties of
362 Hydro-ecological Corridors) of the PIREN Seine research program (2015-2019).

363

364 **6- Data availability**

365 In order to access the data, we kindly ask researchers to contact the corresponding author.

366

367 **7- Acknowledgement**

368 This research was supported by the PIREN Seine research program. We extend our warm
369 thanks to Christelle Sanchez for her participation in the geophysical survey.

370 **8- References**

371 Antoine, P., Coutard, J.-P., Gibbard, P., Hallegouet, B., Lautridou, J.-P., Ozouf, J.-C. 2003.
372 The Pleistocene rivers of the English Channel region. *Journal of Quaternary Science*, 18,
373 227–243.

374 Benech, C., Lombard, P., Rejiba, F., and Tabbagh, A. 2016. Demonstrating the contribution
375 of dielectric permittivity to the in-phase EMI response of soils: example of an archaeological
376 site in Bahrain. *Near Surface Geophysics*, 14(4), 337-344.

377 Berger, G., Delpont, G., Dutartre, P., Desprats, J.-F. 1995. Evolution de l'environnement
378 paysager de la vallée de la Seine - Cartographie historique et prospectives des explorations
379 alluvionnaires de la Bassée. *French Geological Survey (BRGM) report R 38 726*, 39 p.



- 380 Caillol, M., Camart, R., Frey, C. 1977. Synthèse bibliographique sur la géologie,
381 l'hydrogéologie et les ressources en matériaux de la région de Nogent-sur-Seine (Aube).
382 *French Geological Survey (BRGM) report 77 SGN 303 BDP*, 108 p.
- 383 Deleplancque, B. 2016. Caractérisation des hétérogénéités sédimentaires d'une plaine
384 alluviale : Exemple de l'évolution de la Seine supérieure depuis le dernier maximum glaciaire.
385 *PhD Thesis, PSL Research University – Paris*, 273 p.
- 386 Everett, M. E. 2012. Theoretical developments in electromagnetic induction geophysics with
387 selected applications in the near surface. *Surveys in geophysics*, 33(1), 29-63.
- 388 Flipo, N., Mouhri, A., Labarthe, B., Biancamaria, S., Rivière, A., Weill, P. 2014. Continental
389 hydrosystem modelling: the concept of nested stream-aquifer interfaces. *Hydrology and Earth*
390 *System Sciences*, 18, 3121–3149.
- 391 Guptasarma, D., and B. Singh, 1997, New digital linear filters for Hankel J0 and J1
392 transforms: *Geophysical Prospecting*, 45, no. 5, 745–762.
- 393 Jordan, D.W., Prior, W.A. 1992. Hierarchical Levels of Heterogeneity in a Mississippi River
394 Meander Belt and Application to Reservoir Systems: Geologic Note. *AAPG Bulletin*, 76(10),
395 1601-1624.
- 396 Lavoué, F., Van Der Kruk, J., Rings, J., André, F., Moghadas, D., Huisman, J. A., Lambot, S,
397 Weihermüller, L., Vanderborght, J., and Vereecken, H. 2010. Electromagnetic induction
398 calibration using apparent electrical conductivity modelling based on electrical resistivity
399 tomography. *Near surface geophysics*, 8(6), 553-561.
- 400 Loke M.H., Acworth I. and Dahlin T. 2003. A comparison of smooth and blocky inversion
401 methods in 2D electrical imaging surveys. *Exploration Geophysics* **34**, 182–187.



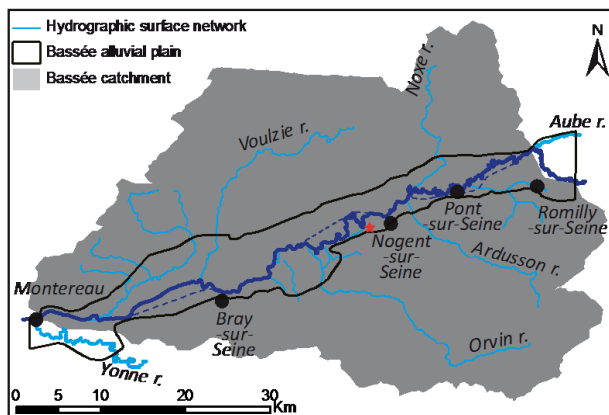
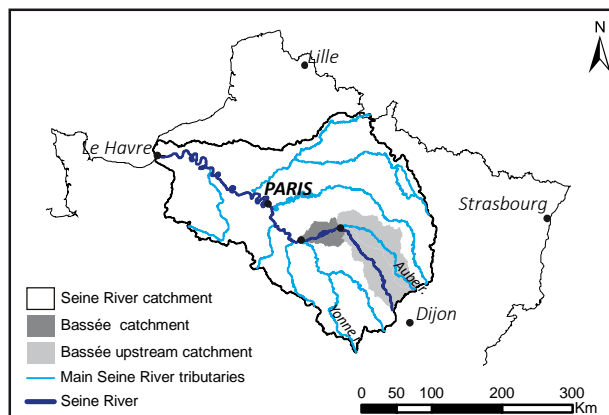
- 402 Mégnien, F. 1965. Possibilités aquifères des alluvions du val de Seine entre Nogent-sur-Seine
403 et Montereau, incluant la carte géologique et géomorphologique de la Bassée. *French*
404 *Geological Survey (BRGM) report 65-DSGR-A-076*, 452 p.
- 405 Miall, A.D. 1988. Reservoir Heterogeneities in Fluvial Sandstones: Lessons from Outcrop
406 Studies. *AAPG Bulletin*, 72(6), 682-697.
- 407 Mordant, D. 1992. La Bassée avant l'histoire : archéologie et gravières en Petite-Seine.
408 *Association pour la promotion de la recherche archéologique en Ile-de-France*, Nemours,
409 143 p.
- 410 Nabighian, M. N. (Ed.). 1988. *Electromagnetic methods in applied geophysics* (Vol. 2). SEG
411 Books.
- 412 McNeill, J. D. 1980. Electromagnetic terrain conductivity measurement at low induction
413 numbers. *Geonics Technical Note TN-6*.
- 414 Pastre, J.-F., Limondin-Lozouet, N., Leroyer, C., Ponel, P., Fontugne, M. 2003. River system
415 evolution and environmental changes during the Lateglacial in the Paris Basin (France).
416 *Quaternary Science Reviews*, 22, 2177–2188.
- 417 Spies, B. R. 1989. Depth of investigation in electromagnetic sounding
418 methods. *Geophysics*, 54(7), 872-888.
- 419 Schamper, C., Rejiba, F., and Guérin, R. 2012. 1D single-site and laterally constrained
420 inversion of multifrequency and multicomponent ground-based electromagnetic induction
421 data — Application to the investigation of a near-surface clayey
422 overburden. *Geophysics*, 77(4), WB19-WB35.



- 423 Simon, F. X., Sarris, A., Thiesson, J., & Tabbagh, A. 2015. Mapping of quadrature magnetic
424 susceptibility/magnetic viscosity of soils by using multi-frequency EMI. *Journal of Applied*
425 *Geophysics*, 120, 36-47.
- 426 Tabbagh, A. 1986. Applications and advantages of the Slingram electromagnetic method for
427 archaeological prospecting. *Geophysics*, 51(3), 576-584.
- 428 Thiesson, J., P. Kessouri, C. Schamper, and A. Tabbagh. 2014. About calibration of frequency
429 domain electromagnetic devices used in near surface surveying. *Near Surface Geophysics*, 12,
430 481–491.
- 431 Wannamaker, P. E., Hohmann, G. W., and Sanfilipo, W. A. 1984. Electromagnetic modeling
432 of three-dimensional bodies in layered earths using integral equations. *Geophysics*, 49, 60–74,
433 doi: 10.1190/1.1441562.
- 434 Ward, S. H., and Hohmann, G. W. 1988. Electromagnetic theory for geophysical
435 applications. *Electromagnetic methods in applied geophysics*, 1(3), 131-311.
- 436 Xiong, Z. 1989. Electromagnetic fields of electric dipoles embedded in a stratified anisotropic
437 earth. *Geophysics*, 54, 1643–1646, doi: 10.1190/1.1442633.
- 438



439 **Figures**



440

441 Figure 1: maps of the Seine catchment (top) and the Bassée alluvial plain.



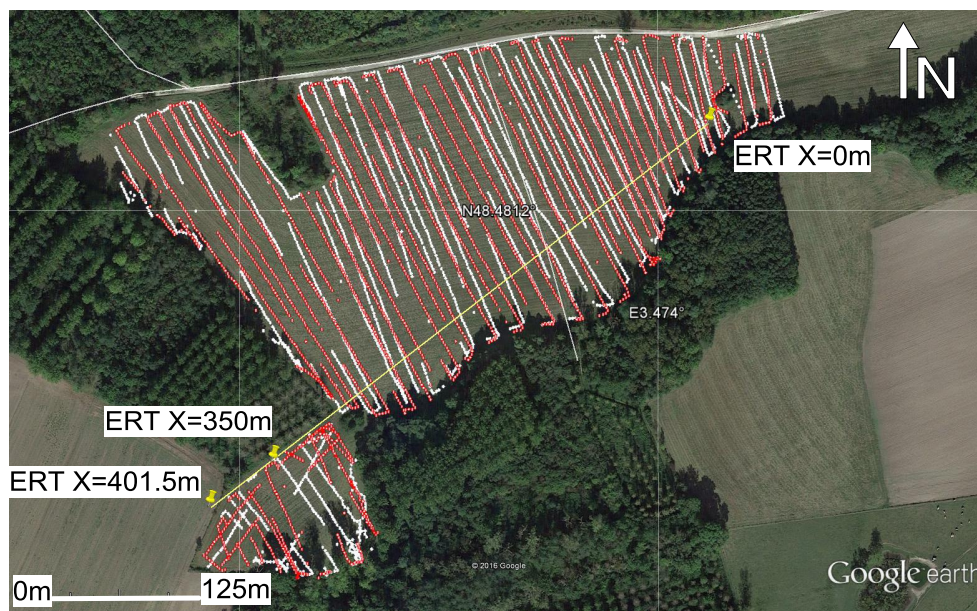
442

443 Figure 2 : LIDAR map of the studied area, showing the contemporary location of the Seine
444 river, together with the narrow and wide paleochannel interpretations.

445



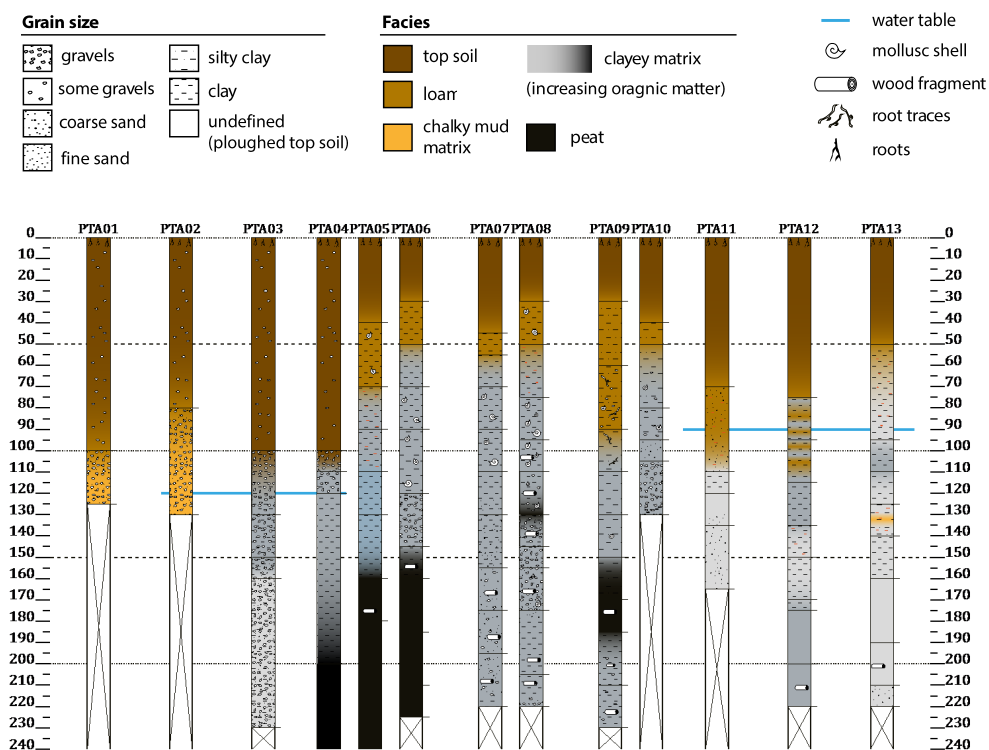
446



447

448 Figure 3: Map of the surveyed area, showing the loci of the VCP (red) and HCP (white)
449 measurements. The reference (ERI) profile, recorded with a Wenner-Schlumberger
450 configuration using 1 m electrode spacing between 0 and 350 m, and a 0.5 m electrode
451 spacing between 350 m and 401.5 m, is indicated by the yellow line.

452



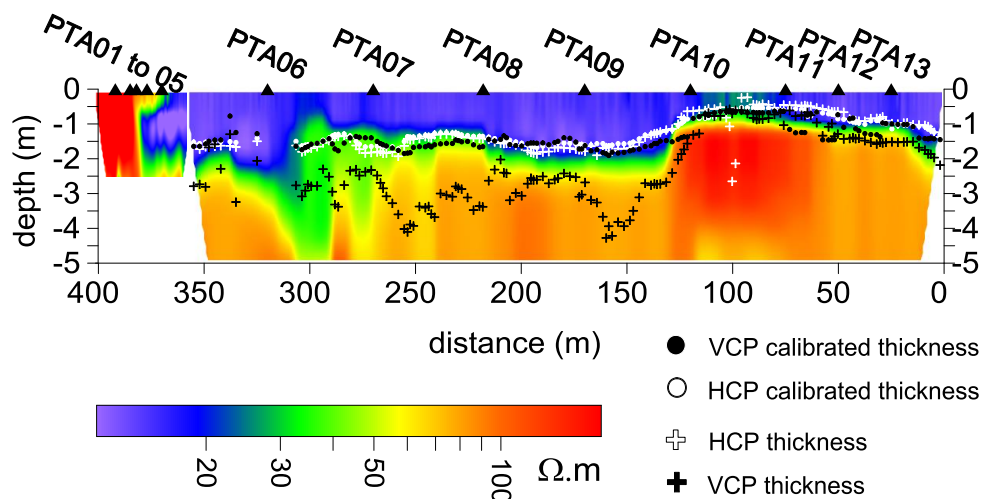
453

454 Figure 4: log of hand auger soundings performed along the reference profile. The position of
 455 each sounding along the ERI profile is shown in Figure 5.

456

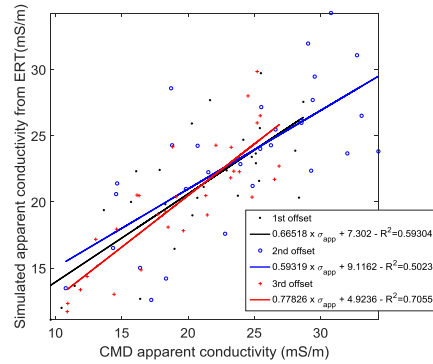
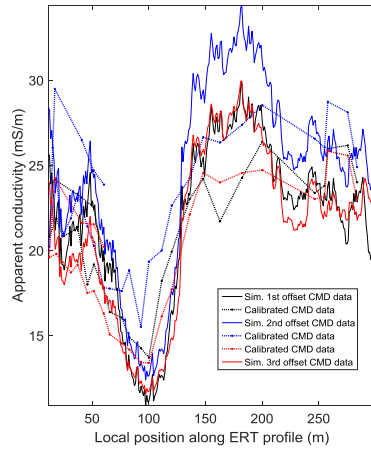


457

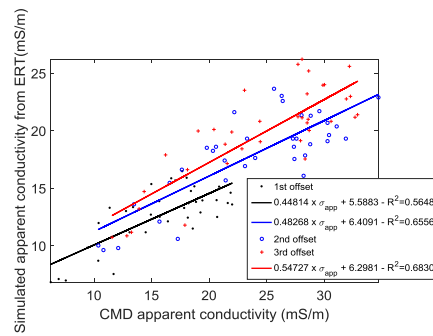
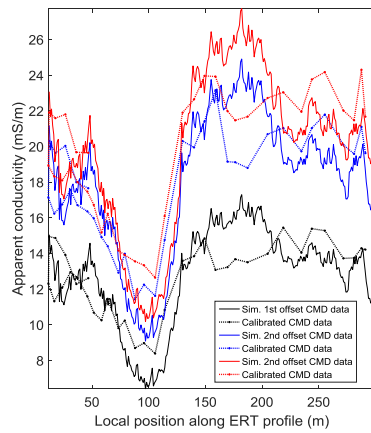


458

459 Figure 5: Results from the electrical resistivity tomography (ERI) inversion, computed along
460 the reference profile. This map clearly reveals the two main (conductive and resistive)
461 geological units. The markers correspond to the inverted loci of the interface between the
462 conductive unit and the substratum, before and after linear calibration (Figure 6). This figure
463 shows that calibration of the raw VCP measurements leads to significant corrections in
464 inverted depth, when compared to the calibration of the HCP measurements.



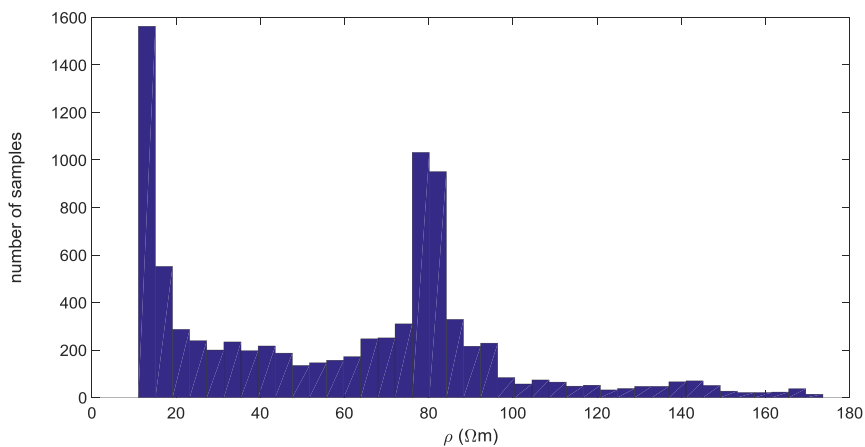
465



466

467 Figure 6: HCP (top) and VCP (bottom) calibration results obtained along the reference
 468 profile. Left: the simulated apparent CMD conductivities based on ERI inversion compared
 469 to the calibrated EMI measurements. Right: scatter plot of the measured vs simulated apparent
 470 conductivities. The solid lines indicate the corresponding linear regressions.

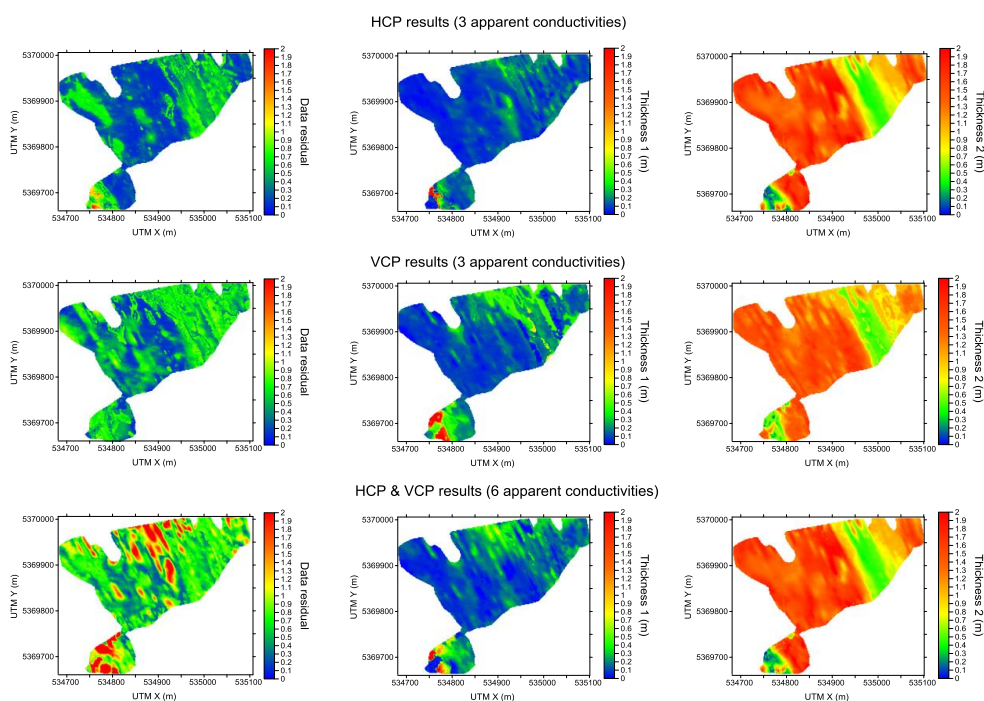
471



472

473 Figure 7: histogram of the electrical resistivity values determined for the tomographic cross
474 section shown in Figure 5.

475



476

477 Figure 8: Results of the CMD inversion, including the data residual (left column), for a three-
 478 layer model (1: topsoil, 2: conductive filling, and 3: resistive substratum). The thicknesses 1
 479 and 2 correspond to the topsoil and conductive filling, respectively. The prospection height is
 480 1 m. The conductivities are set to $\sigma_1 = 13$ mS/m, $\sigma_2 = 72$ mS/m and $\sigma_3 = 13$ mS/m. A noise
 481 level of 1 mS/m on the apparent conductivities was assumed, with a minimum relative error
 482 of 5%.

483